Proc. Natl. Acad. Sci. USA
Vol. 89, pp. 236–240, January 1992
Neurobiology

Computational model of the on-alpha ganglion cell receptive field based on bipolar cell circuitry

(retina/neural circuitry/neural modeling/neural network)

MICHAEL A. FREED*†, ROBERT G. SMITH‡, AND PETER STERLING‡

*Laboratory of Neurophysiology, National Institute of Neurological Disorders and Stroke, Building 36, Room 2C02, National Institutes of Health, Bethesda, MD 20892; and ‡Department of Anatomy, University of Pennsylvania, Philadelphia, PA 19104

Communicated by Robert H. Wurtz, September 5, 1991

ABSTRACT **The on-alpha ganglion cell in the area centralis of the cat retina receives ≈450 synapses from type b_1 cone bipolar cells. This bipolar type forms a closely spaced array (9 μm), which contributes from 1 to 7 synapses per b_1 cell throughout the on-alpha dendritic field. Here we use a compartmental model of an on-alpha cell, based on a reconstruction from electron micrographs of serial sections, to compute the contribution of the b_1 array to the on-alpha receptive field. The computation shows that, for a physiologic range of specific membrane resistance (9500–68,000 Ω·cm²) and a linear synapse, inputs are equally effective at all points on the on-alpha dendritic tree. This implies that the electrotonic properties of the dendritic tree contribute very little to the domed shapes of the receptive field center and surround. Rather, these shapes arise from the domed distribution of synapses across the on-alpha dendritic field. Various sources of "jitter" in the anatomical circuit, such as variation in bipolar cell spacing and fluctuations in the number of synapses per bipolar cell, are smoothed by the overall circuit design. However, the computed center retains some minor asymmetries and lumps, due to anatomical jitter, as found in actual alpha-cell receptive fields.**

The receptive fields of both on and off types of alpha (Y) ganglion cells are tuned to low spatial frequencies (cutoff frequency, 2 c/degree in area centralis) (1). The Y cell contributes the major retinal input to area 18, which may explain the low-frequency tuning of this area (2, 3). The alpha cell's contribution to the visual system depends critically on the structure of its receptive field. There are two overlapping regions: a relatively broad center and a still broader antagonistic surround, each with a roughly Gaussian distribution of sensitivity (4–7).

The question we address here is how does the alpha (Y) receptive field structure arise from retinal circuitry? Analytical models of the alpha receptive field give some important clues (8–11). Such models, as schematized in Fig. 1, hypothesize the receptive field to arise from a pooling of linear subunits. Each linear subunit has a center and surround with Gaussian distributions of sensitivity. These linear subunits are weighted individually and summed in a linear fashion. If appropriate distributions of sensitivity for the subunits are chosen, as well as the correct weightings, then the summed subunit centers duplicate the alpha center and the summed subunit surrounds duplicate the alpha surround (8). Although correspondence has not been established between linear subunits and any particular elements of retinal circuitry, they closely resemble, by their individual properties and their array, the bipolar cells that contact the on-alpha cell. We had previously described this source of input by reconstructing an on-alpha cell from serial, electron microscopic sections. Most bipolar synapses (82–89%) derive from a single bipolar type, denoted b_1. The b_1 cell, like the hypothetical linear subunit, forms a regular, closely spaced array across the retina (average distance to nearest neighbor, 9 μm) (12) and its receptive field has a center and surround (13).

Here we combine the general structure of the analytical models with detailed anatomical data to compute the contribution of the b_1 array to the on-alpha receptive field. The computation assumes, like the analytical models, that the on-alpha cell sums its inputs linearly. Although there are temporal nonlinearities within the on-alpha receptive field, given moderate stimulus contrast, these nonlinearities apparently sum in a spatially linear fashion (9, 11). The computation also assumes that every b_1 synapse evokes the same conductance increase in the on-alpha cell (for a given depolarization of the bipolar cell) and that this conductance increase depolarizes the on-alpha cell. These assumptions simplify the computation of the on-alpha receptive field to a weighted summation of bipolar receptive fields. A bipolar cell's weight depends on the number of synapses it contributes to the on-alpha dendrites and the electrotonic effects of these synapses at the soma.

METHODS

An on-alpha ganglion cell from the area centralis had been filled with horseradish peroxidase, blackened with diaminobenzidine, and drawn with a camera lucida (12). Almost half of the dendritic arbor, spanning the full-field diameter, had been reconstructed by electron microscopy (shaded area in Fig. 2). The dendritic tree had 9 orders of bifurcation, which produced 123 branches. We measured branch diameters at 3-μm intervals from the reconstruction and at 6-μm intervals from the camera lucida drawing, noting an average diameter and length for each branch. The light and electron microscope measurements disagreed slightly; the standard error for the difference of their means was ≈0.1 μm. Since the electron microscope measurements were presumably more accurate than the camera lucida measurements, they were used in preference to the light microscope measurements. The latter were used when a branch extended beyond the reconstructed area.

These measurements were incorporated into a compartmental model of the on-alpha cell, including synaptic input (14–16) (Fig. 2). Each branch was represented as a series of isopotential compartments, all with the average diameter of the branch. The length of each compartment was chosen to be 1/10th of the branch's space constant $(D \cdot R_m/4 \cdot R_i)^{1/2}$ (17). One compartment from each branch was halved and placed at each end of the branch. To join a parent branch with its two daughters, their three terminal compartments were added to shape a single compartment (see Fig. 2 *Inset*).

A compartment consisted of a membrane resistance (r_m) in series with a leakage potential ($E_m = -70$ mV) and a variable

The publication costs of this article were defrayed in part by page charge payment. This article must therefore be hereby marked "*advertisement*" in accordance with 18 U.S.C. §1734 solely to indicate this fact.

†To whom reprint requests should be addressed.

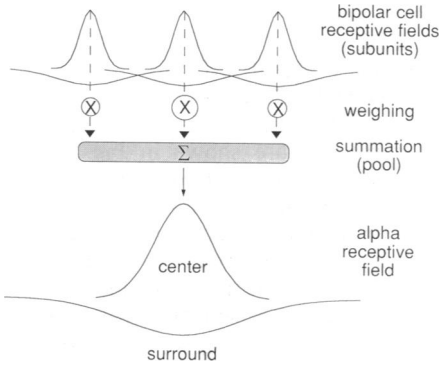

FIG. 1. Schematic of the computation based on neural components. Structure resembles that of previous abstract models of the alpha receptive field using hypothetical components (in parentheses).

synaptic conductance (r_s) in series with a synaptic battery (E_s = 0 mV; see Fig. 2 *Inset*) (16). Each compartment was connected by cytoplasmic resistance (r_i) to the next compartment (R_i = 100 Ω·cm).

Each compartment's membrane resistance was calculated from its diameter and length by using a specific membrane resistance (R_m) of 9500 Ω·cm^2. This value was taken from whole cell recordings of dissociated rat retinal ganglion cells (18). A similar value was derived by one of us (19) under conditions of bright mesopic illumination from intracellular recordings of on-alpha cells. These recorded cells resembled the reconstructed cell in location, morphology, and size. Their input impedances were ≈120 MΩ. To duplicate this input impedance at the soma, the compartmental representation of the on-alpha cell required a specific membrane resistance of 9500 Ω·cm^2. Higher values for specific membrane resistance (68,000 Ω·cm^2) have been reported for retinal ganglion cells in the amphibian *Necturus* (20). This may be due to a difference of species and/or temperature (21). Still, we tested the effect of this higher membrane resistance (see *Results*).

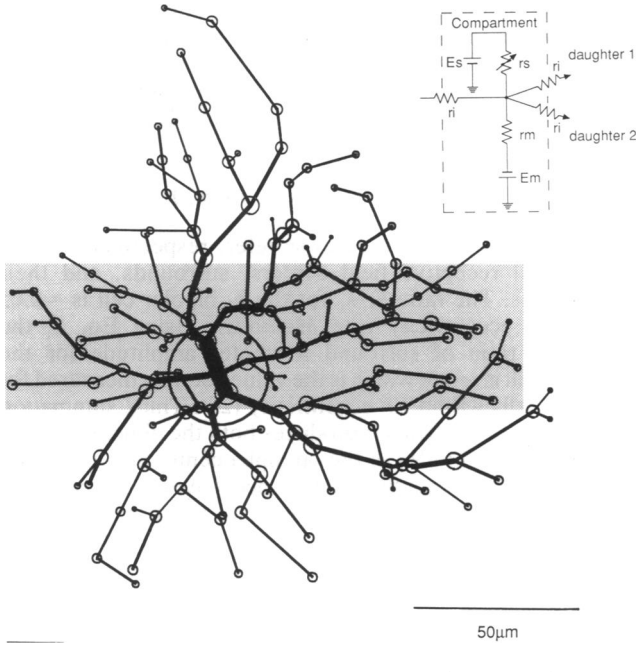

FIG. 2. Compartmental representation of the on-alpha cell. Branches are divided into compartments (circles); many of these are terminal compartments shared by three branches. The size of each compartment is shown by its diameter, which is the diameter of a sphere with equivalent resistance (r_m) and capacitance (c_m). Shaded area indicates reconstructed portion (40%) of dendritic arbor. (*Inset*) Battery-resistor representation of a compartment. The terminal compartment of a branch is joined by an axial resistance (r_i) to another compartment at left and by 2 axial resistances to daughter branches at right.

The value chosen for synaptic conductance was constrained by the assumption of linearity. This requires the synaptic conductance to be small compared to the ganglion cell's input conductance (reciprocal of input resistance) at the point of synapsis (15). Thick dendritic branches near the soma would have input conductance as high as 8×10^{-9} S, but at the edge of the dendritic field thin branches would have input conductances as low as 1×10^{-9} S. Thus, for a bipolar synapse to operate linearly everywhere in the dendritic field, its conductance must be even lower, on the order of 1×10^{-10} S. This choice of conductance for the computation ensures that synapses on the thinnest and thickest branches would depart from linearity by no more than 1–9% (from equation 2.12 of ref. 22). Since a linear synapse approximates a current source, we also used a current injection to simulate the synapse and to provide a benchmark for linear operation.

The program NEURONC was used to calculate the voltage at each branch point in the dendritic tree during a simulated synaptic input: either current injection, voltage clamp, or change in conductance. The voltage within every compartment was found by calculating current flow through its membrane resistance and from neighboring compartments using Kirchoff's and Ohm's laws. Since the voltage in a given compartment depended on the voltage within all other compartments, the voltage computations were iterated over compartments by a method of successive approximation to within a criterion voltage (1×10^{-8} V) (23). A steady-state computation was made because the period of the stimulus used to map the on-alpha receptive field (>500 msec) was much longer than the time constant of the cell itself (10 msec).

The computations used values of 80 and 150 μm, respectively, for the Gaussian radii of the on-alpha receptive field center (r_c) and surround (r_s) and 30 and 130 μm, respectively, for the Gaussian radii of the b_1 receptive field center and surround. Recordings from b_1 bipolar cells have been accomplished infrequently (13), but on theoretical grounds the on-beta ganglion cell receptive field should have the same dimensions as that of the b_1 bipolar cell and can be used in its stead (24). We derived the values for the on-alpha and on-beta cells as follows: at 1° eccentricity, the receptive field center diameter (span between loci where the spike rate response falls to spontaneous level) is ≈0.7° for the on-alpha cell and ≈0.3° for the on-beta cell (1). We converted center diameter to r_c by noting that the center diameter overestimates r_c by a factor of 2.06 for on-alpha cells and 2.6 for on-beta cells, where both have been measured at the same location (1, 25) (see ref. 26 for an explanation). Therefore, r_c for the on-alpha and on-beta cells equaled their center diameters divided by these factors and converted to a linear measurement over the retinal surface (27). The parameter r_s was taken as 1.9 and 4.3 times r_c for the on-alpha and on-beta, respectively (within 10° eccentricity; ref. 25). As predicted, the resulting values for the on-beta cell receptive field agree with the smallest b_1 receptive field obtained by direct measurements (13, 28).

RESULTS

Electrotonic Effects of a Linear Synapse. When a single bipolar synapse was simulated as a low synaptic conductance (1×10^{-10} S), or a current injection (1×10^{-11} A), the effect on local voltage is the same everywhere in the dendritic field (see *Methods*). Our first step was to determine the effect of synapses at various dendritic loci on the voltage at the soma. Therefore, we simulated a synapse at each branch point and computed the effect on soma voltage (Fig. 3). For both conductance and current simulations, the effect of a synapse

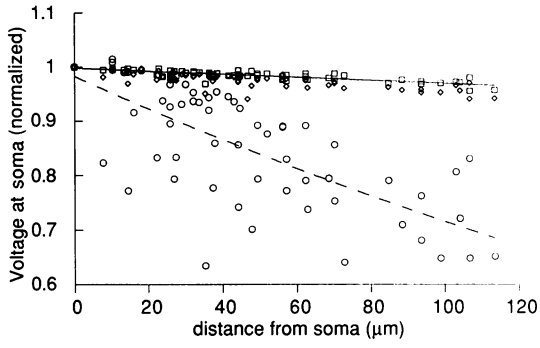

FIG. 3. Effect of synapses at different locations within reconstructed portion of dendritic tree on soma voltage. A synapse was simulated by current injection (squares), a saturating synaptic conductance (circles), or a nonsaturating synaptic conductance (diamonds). The resulting soma voltage was normalized to the effect of a synapse at the soma. Distance is measured across retinal surface. The results of the saturating synaptic conductance and the current injection are fitted by exponentials with space constants, respectively, of 315 and 3450 μm.

at the edge of the dendritic field was almost the same (within 3%) as one at the soma. Differences between the conductance and the current simulations were slight and produced no discernible effect on the computation of the on-alpha receptive field. Thus, for a linear synapse the distribution of synaptic effect is virtually uniform across the dendritic field.

Weighting and Summing the Bipolar Cells. The next step was to determine the appropriate weighting for the individual b_1 bipolar cells whose synaptic contacts on the alpha dendritic tree had been determined. The reconstructed portion of the dendritic field encompassed 74 b_1 axons and 62 of these contacted the alpha cell. Synapses from a given axon usually clustered on the alpha dendritic tree, often near a branch point (see figure 6 of ref. 12). Therefore, at the branch point nearest to the synaptic contacts of a given bipolar cell, we injected current and calculated the effect on soma voltage. This voltage was normalized to the effect of a synapse at the soma and assigned to each bipolar cell as its electrotonic weight. The total weight of a bipolar cell was this electrotonic weight times the number of synapses it contributed to the ganglion cell.

The weighting of each b_1 axon terminal within the reconstructed portion of the on-alpha dendritic tree showed considerable local variation (Fig. 4*A*). However, a global maximum occurred near the middle of the dendritic field where, on the average, more synapses per bipolar cell contacted the alpha cell. To determine the contribution of the b_1 array to the on-alpha receptive field, we summed the b_1 receptive fields, centering them on the physical location of the axon terminals, and scaling them by the weighting belonging to each bipolar cell. The b_1 centers and surrounds were summed separately. The summed centers gave a smooth, domed surface (Fig. 4*B*); evidently, b_1 centers are broad enough and closely spaced enough to smooth out most of the discontinuous, noisy distribution of bipolar cell weights. The summed surrounds gave a still broader, domed surface.

Computing On-Alpha Center and Surround. Vertical slices through the domed surfaces of the summed bipolar cell centers and surrounds are shown in Fig. 5*A* (solid line). Receptive fields of bipolar cells outside the reconstructed region were omitted from the summation, but since the slices were centered on the reconstructed region and parallel to it, this omission is inconsequential. The peak of the center summation was asymmetrical with a slight declivity to the right. These irregularities arise from local peaks and declivities in the concentration of synapses (Fig. 4*A*). The surround summation was smooth and without such irregularities. The estimated best fits to the on-alpha receptive field center and surround in the region of the reconstructed cell are Gaussians with radii (r_c, r_s), respectively, of 80 and 150 μm (see *Methods*). These are shown superimposed on the bipolar summations (Fig. 5*A*, dashed line). The matches are fairly good, especially compared to the range of alpha receptive field sizes across the retina: alpha centers can be as wide as 650 μm and alpha surrounds can be as wide as 700 μm (25).

To see the effect of the bipolar cell weightings across the field on the receptive field center and surround (Fig. 4*A*), we repeated the summations, giving every bipolar cell equal weight. The resulting center summation was markedly flattened on top and slightly broader at half-amplitude (Fig. 5*D*, thin dashed line), but the surround summation was hardly affected.

The ratio of surround to center amplitude was determined analytically in a separate computation. This was necessary because the bipolar cells outside the reconstructed region, which were omitted from the summations of Figs. 4*B* and 5*A*, would affect this ratio. Because the bipolar cell centers, surrounds, and also their summations are all Gaussian, their integrals can all be described by the formula: $\pi k r_n^2$ where k represents peak sensitivity and r_n is the Gaussian radius. When summing equal numbers of centers and surrounds, the ratio of the integrals of the center and surround equals the ratio of the integrals of their summations. This leads to the equation

$$k_{ss}/k_{cs} = (k_s \cdot r_s^2 \cdot r_{cs}^2)/(k_c \cdot r_c^2 \cdot r_{ss}^2), \quad [1]$$

where subscripts c, s, cs, and ss refer, respectively, to the bipolar cell receptive field centers, surrounds, and their summations. The ratio k_s/k_c for the b_1 bipolar cell is ≈0.05 within 10° eccentricity (see *Methods*). Using Eq. **1**, the calculated ratio of surround to center amplitude for the on-alpha cell is ≈0.3, which is the value actually measured for on-alpha cells within 10° eccentricity (25). Thus, summation of the b_1 receptive fields reproduces both the dimensions and the relative amplitudes of the on-alpha center and surround.

Effect of High Synaptic Conductance. Given a computation that approximates the actual on-alpha receptive field, we

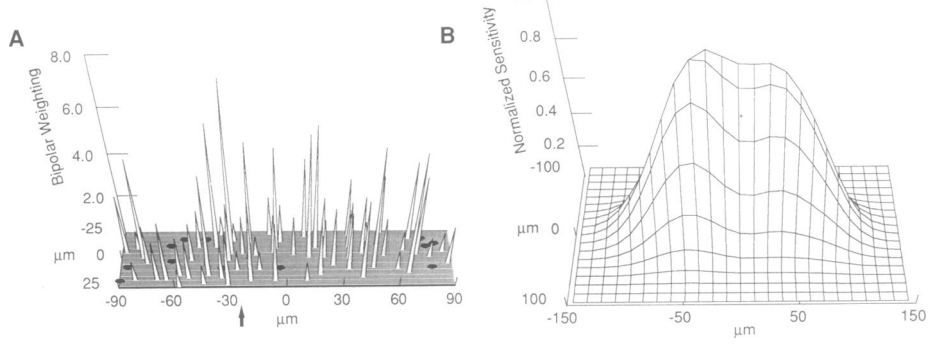

FIG. 4. Bipolar cell contribution to on-alpha receptive field center. (*A*) Weighting (needle height) and position (needle location) of 62 b_1 bipolar cells that contacted the on-alpha cell with the reconstructed portion of its dendritic arbor. Twelve bipolar cells (black holes) were within the reconstructed portion but did not contact the alpha cell. The greatest weightings occurred over the position of the soma (arrow). (*B*) The summation of b_1 bipolar cell receptive field centers using weighting in *A*.

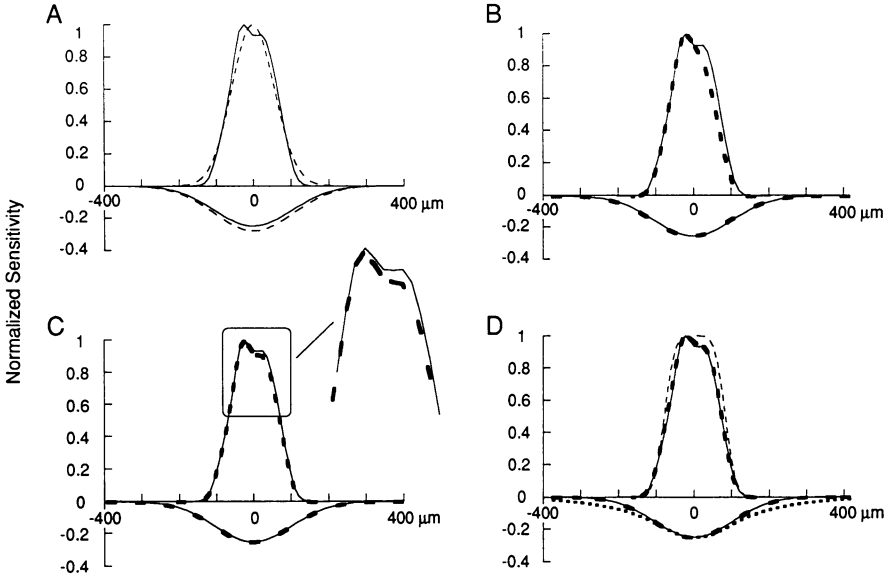

FIG. 5. Slices through the middle of summed bipolar cell contributions to on-alpha center (above abscissa) and surround (below abscissa). (*A–D*) Summation using best estimate of specific membrane resistance (R_m = 9500 Ω·cm^2) and assuming linear synaptic operation is indicated by a solid line. This best estimate is compared to Gaussian distribution fit to actual on-alpha center and surround (*A*), center and surround summations using saturating synaptic conductance (2.5×10^{-9} S) (*B*), center and surround summation using R_m = 2500 Ω·cm^2 (*C*), center and surround summations weighting each bipolar cell by number of contributed synapses (heavy dashed line) or equally weighting and spacing all bipolar cells (thin dashed line) and surround summation using an exponential function to represent the bipolar surround (heavy dotted line) (*D*).

could study the effect of varying the electrotonic characteristics of the dendritic tree. One variation might occur naturally when the receptive field is plotted with a light spot of saturating intensity. Then the resulting synaptic currents might exceed the linear range of the synapse (see *Methods*).

With a high synaptic conductance (2.5×10^{-9} S), the effect of a synapse on soma voltage was no longer flat across the field (Fig. 3, open circles). Now the distribution of amplitudes across the dendritic field was quite uneven. Moreover, distal synapses contributed much less voltage to the soma than proximal synapses (≈30% less). This gradient arises from the distribution of input resistances, which are highest at the edge of the dendritic field where the dendrites are finest. High input resistance, coupled with high synaptic conductance, saturates the synapse, thus reducing synaptic efficacy at the dendritic field edge (15). Using the high synaptic conductance, we recomputed the contribution of the b_1 array to the on-alpha receptive field (Fig. 5*B*). The summation of b_1 centers was now more symmetrical and the declivity disappeared (Fig. 5*B*, dashed line). The shape of the surround summation was unaffected.

Effect of Membrane Resistance. Different levels of background luminance may evoke different levels of tonic synaptic input to the on-alpha cell, and this could alter the membrane resistance. To explore this effect, we decreased the R_m to 2500 Ω·cm^2 and repeated the computation (Fig. 5*C*, dashed line). The center summation differed slightly in shape from the summation using our best estimate of R_m (9500 Ω·cm^2). Increasing the R_m to 68,000 Ω·cm^2 gave a center summation indistinguishable from that when the best estimate was used. The shape of the surround was unchanged by either variation. These results accord with the observation that over a wide luminance range (photopic-mesopic), receptive field structure is independent of background (29, 30).

The effects of varying the membrane resistance suggested that the shape of the receptive field center depends very little on the electrotonic properties of the dendritic tree. To confirm this, we eliminated these electrotonic properties from the summations altogether, weighting each bipolar cell solely by the number of synapses it contributed. The resulting summations were very close to the summations using the best estimate of specific membrane resistance (Fig. 5*D*, heavy dashed line).

DISCUSSION

The present computation based on the b_1 bipolar cell–on-alpha circuit accurately simulates the spatial properties of the on-alpha receptive field. The computation is congruent with previous abstract models of the alpha receptive field that specify the linear summation of subunits (8–11). Therefore, it affirms these models and indicates that the b_1 bipolar circuit is sufficient for the on-alpha receptive field. Moreover, this circuit is probably necessary for the receptive field: the drug 2-amino-4-phosphonobutyrate, which blocks on-bipolar cells (31), such as the b_1 cell, also blocks or drastically reduces all components of the on-alpha response (32, 33). Thus, a ganglion cell receptive field is "explained" mechanistically by the interaction between a defined input circuit and the cell's intrinsic, biophysical properties. To our knowledge, this is the first example, in a vertebrate, of such an explanation at this level of neural organization (see also ref. 34).

The model provides an important tool for investigating various features of the circuit. For example, the simulations show that the electrotonic structure of the alpha dendritic tree contributes almost nothing to the form of the receptive field. The reason is that a b_1 excitatory postsynaptic current (epsc) decays very little on the way to the soma, even if it arises at the most distal tip of an alpha dendrite. This conclusion holds for a wide range of physiologically plausible values of R_m for the alpha cell: 9500–68,000 Ω·cm^2. Even for an extremely low value (R_m = 2500 Ω·cm^2), the average decay of an epsc from dendritic tip to soma is only 15%. The effect of such a small decrement would be unnoticed in the extent and form of the alpha receptive field because other parameters dominate.

The simulations show the most important contribution to the domed peak of the receptive field center to be the peaked distribution of b_1 synapses across the alpha dendritic field. Omitting this feature flattens the peak. However, this same parameter hardly affects the surround; in fact only one of the parameters that were varied in the present simulations much affected the surround (Figs. 4 and 5). The explanation is simple: the alpha surround is a convolution of the broad b_1 surround with a narrow synaptic weighting function. In such an operation, the shape of the broader distribution predominates. However, when the b_1 surround is represented as an exponential (instead of a Gaussian), then the form of the alpha surround was indeed altered (Fig. 5*D*, heavy dotted line).

An important point emerging from the simulation is that the conductance modulated by a single bipolar synapse cannot much exceed 100 pS if the on-alpha cell is to operate in a linear fashion (see *Methods*). Since the unit conductance of a transmitter-gated ion channel is >10 pS (35) (for mammalian

ganglion cells, see refs. 18 and 20), a single bipolar synapse might modulate as few as 10 channels. Similar numbers of channels (13–20) are opened by single quanta of transmitter at other central nervous system synapses (36, 37). About 450 b_1 synapses contact the alpha cell (12). Were all these synapses to release single quanta simultaneously (as might be expected, for example, to a low-contrast stimulus filling the receptive field center) the resulting conductance would be >45,000 pS. Such an increase seems impossibly large since it would profoundly saturate the alpha cell simulated here. The largest input conductance measured for an on-alpha cell during low-contrast stimulation is <10,000 pS (19). This seems to suggest that, under such conditions, the probability of release at each bipolar synapse is considerably less than 1. Such an idea is certainly consistent with findings at other central synapses (38, 39).

The anatomical circuit contains various sources of jitter: irregularities in the b_1 bipolar cell spacing; "holes" due to b_1 cells in the alpha dendritic field that contribute no contacts; local variation in the number of contacts per b_1 cell to the alpha cell (Fig. 4). The computation indicates that much of this jitter disappears in the summation. The close spacing of these bipolar cells, coupled with their broad receptive fields, causes an averaging that smooths the distribution of sensitivity across the on-alpha receptive field.§ Thus, the circuit's overall design, closely spaced arrays of broad-field elements, serves to relax the anatomical precision with which it need be wired. However, a residual asymmetry remains at the peak of the computed alpha center, arising from local fluctuation in the number of synapses contributed by each bipolar cell (Fig. 5). Comparable asymmetries, including an asymmetrical peak over the soma, have actually been observed in maps of on-alpha receptive fields (6, 26, 40). Probably these small irregularities are smoothed at the next stage of convergence.

In addition to the large center and surround, the on-alpha receptive field includes an array of smaller nonlinear subunits, characterized by their rectifying response (11). A previous compartmental model of an alpha cell (22) based on a low specific membrane resistance (2500 $\Omega \cdot cm^2$) suggested that nonlinear subunits correspond to discrete regions of the alpha dendritic tree. This scheme is unlikely, however, since the subunits coalesce into a single large subunit as the specific membrane resistance approaches currently published values (>8000 $\Omega \cdot cm^2$) (19, 20, 22). A more plausible model is a rectifying amacrine cell interposed between the bipolar cell and the ganglion cell. By action of this amacrine cell, each bipolar receptive field would be rectified to form a nonlinear subunit. The proposed correspondence between the rectified bipolar receptive field and the nonlinear subunit is supported by both physiological and anatomical evidence: (*i*) the size and number of nonlinear subunits in an alpha receptive field match those of the bipolar receptive field array (8, 9), (*ii*) rich, direct amacrine synaptic input to the on-alpha cell (12, 41–43), (*iii*) specific identified types of rectifying amacrine cell (44). Yet, it is not known which types of amacrine cell synapse on the on-alpha cell or whether these types include an amacrine cell with rectifying properties.

§Similarly, the b_1 receptive field itself is the weighted sum of five closely spaced, broad, cone receptive fields (24, 28).

This study was supported by National Institutes of Health Grant EY 00828.

1. Cleland, B. G., Harding, T. H. & Tulunay-Keesey, U. (1979) *Science* **205**, 1015–1017.
2. Pasternak, T., Horn, K. & Maunsell, J. H. R. (1989) *Invest. Ophthalmol. Visual Sci.* Suppl. **30**, 426.
3. Ferster, D. (1990) *Visual Neurosci.* **4**, 135–145.
4. Kuffler, S. W. (1953) *J. Neurophysiol.* **16**, 37–68.
5. Barlow, H. (1953) *J. Physiol. (London)* **119**, 69–88.
6. Rodieck, R. & Stone, J. (1965) *J. Neurophysiol.* **28**, 833–849.
7. Enroth-Cugell, C. & Robson, J. (1966) *J. Physiol. (London)* **187**, 517–552.
8. Enroth-Cugell, C. & Freeman, A. W. (1987) *J. Physiol. (London)* **384**, 49–79.
9. Victor, J. D. & Shapley, R. M. (1979) *J. Gen. Physiol.* **74**, 671–689.
10. Cleland, B. G. (1983) *Proc. Aust. Physiol. Pharmacol. Soc.* **14**, 192–201.
11. Hochstein, S. & Shapley, R. M. (1976) *J. Physiol. (London)* **262**, 265–284.
12. Freed, M. A. & Sterling, P. (1988) *J. Neurosci.* **8**, 2303–2320.
13. Nelson, R. & Kolb, H. (1983) *Vision Res.* **23**, 1183–1195.
14. Cooley, J. W. & Dodge, F. A. (1966) *Biophys. J.* **6**, 587.
15. Rall, W. (1967) *J. Neurophysiol.* **30**, 1138–1168.
16. Joyner, R. W., Westerfield, M., Moore, J. W. & Stockbridge, N. (1978) *Biophys. J.* **22**, 155–170.
17. Perkel, D. H. & Mulloney, B. (1978) *J. Neurophysiol.* **41**, 621–639.
18. Lipton, S. A. & Tauck, D. L. (1987) *J. Physiol. (London)* **385**, 361–391.
19. Freed, M., Nelson, R., Sterling, P. & Smith, R. G. (1991) *Soc. Neurosci. Abstr.* **17**, 344.
20. Coleman, P. A. & Miller, R. F. (1989) *J. Neurophysiol.* **61**, 218–230.
21. Hodgkin, A. L., Huxley, A. F. & Katz, B. (1952) *J. Physiol. (London)* **116**, 424–448.
22. Koch, C., Poggio, T. & Torre, V. (1982) *Philos. Trans. Roy. Soc. London Ser. B* **298**, 227–264.
23. Conte, S. D. & de Boor, C. (1980) *Elementary Numerical Analysis: An Algorithmic Approach* (McGraw-Hill, New York).
24. Smith, R. G. & Sterling, P. (1990) *Visual Neurosci.* **5**, 453–461.
25. Linsenmeier, R. A., Frishman, L. J., Jakiela, H. G. & Enroth-Cugell, C. (1982) *Vision Res.* **22**, 1173–1183.
26. Peichl, L. & Wässle, H. (1979) *J. Physiol. (London)* **291**, 117–141.
27. Bishop, P. O., Kozak, W. & Vakkur, G. J. (1962) *J. Physiol. (London)* **163**, 466–502.
28. Cohen, E. & Sterling, P. (1991) *J. Neurophysiol.* **65**, 352–359.
29. Enroth-Cugell, C., Hertz, B. G. & Lennie, P. (1977) *J. Physiol. (London)* **269**, 297–318.
30. Derrington, A. M. & Lennie, P. (1982) *J. Physiol. (London)* **333**, 343–366.
31. Slaughter, M. M. & Miller, R. F. (1981) *Science* **211**, 182–185.
32. Chen, E. P. C. & Linsenmeier, R. A. (1989) *J. Physiol. (London)* **419**, 77–93.
33. Müller, F., Wässle, H. & Voigt, T. (1990) *J. Neurophysiol.* **59**, 1657–1672.
34. van Hateren, J. H. & Laughlin, S. B. (1990) *J. Comp. Physiol.* **166**, 437–448.
35. Hille, B. (1984) *Ionic Channels of Excitable Membranes* (Sinauer, Sunderland, MA).
36. Ropert, N., Miles, R. & Korn, H. (1990) *J. Physiol. (London)* **428**, 7207–7222.
37. Stuart, G. J. & Redman, S. J. (1990) *J. Physiol. (London)* **420**, 111–125.
38. Korn, H. & Faber, D. S. (1986) in *New Insights into Synaptic Function*, ed. Edeleman, G., Gall, E. & Cowan, M. (Wiley, New York), pp. 57–108.
39. Redman, S. (1990) *Physiol. Rev.* **70**, 165–198.
40. Soodak, R. E., Shapley, R. M. & Kaplan, E. (1991) *Visual Neurosci.* **6**, 621–628.
41. Kolb, H. (1979) *J. Neurocytol.* **8**, 295–329.
42. Nelson, R., Kolb, H., Chandler, N. & DeKorver, L. (1989) *Invest. Ophthalmol. Visual Sci. Suppl.* **30**, 69.
43. Vardi, N., Masarachia, P. & Sterling, P. (1989) *J. Comp. Neurol.* **288**, 601–611.
44. Freed, M. A., Nelson, R., Pflug, R. & Kolb, H. (1990) *Invest. Ophthalmol. Visual Sci. Suppl.* **31**, 114–115.